Eur. Phys. J. D **11**, 127–136 (2000)

**THE EUROPEAN PHYSICAL JOURNAL D**

EDP Sciences


# Simulation of small positively charged MgO clusters and study of their electronic densities

C. Coudray[1,a], G. Blaise[1], and M.J. Malliavin[2]

[1] Laboratoire de Physique des Solides, bâtiment 510, Université Paris-Sud, 91405 Orsay, France
[2] Centre d'Études du Ripault, DMAT/CS/MMH, B.P. 16, 37260 Monts, France

Received 14 September 1999 and Received in final form 2 December 1999

**Abstract.** With the help of *ab initio* methods the clusters $[(MgO)_{13}Mg]^{Q+}$ are simulated for $Q = 0, 1, 2$. Then, vacancy clusters $[(MgO)_{12}Mg_2]^{Q+}$ obtained by removing one oxygen atom are computed for $Q$ running from 0 to 4. These clusters exhibit a slight sphericity and generally shorter interatomic distances than in the crystal. The electronic densities variations are studied in function of $Q$. In particular, it is observed that the electronic density in the oxygen vacancy goes to a maximum when $Q = 2$. The ionisation potentials vary from approximately 4 to 14 eV when $Q$ varies from 0 to 3, with a more rapid increase from $Q = 1$ to $Q = 2$. The stability study of vacancy clusters show that they experience a phase transition when their charge becomes equal to 2, in accordance with the features mentioned above.

**PACS.** 71.24.+q Electronic structure of clusters and nanoparticles – 36.40.Cg Electronic and magnetic properties of clusters – 36.40.Ei Phase transitions in clusters

## 1 Introduction

Over the last few years, there has been strong interest in the study of many oxide clusters [1–11]. Amongst them, singly and doubly charged MgO clusters formed the subject of many experimental and theoretical works [1,2,4–6,9–11]. Thus $(MgO)_n^+$, $(MgO)_nMg^+$, $(MgO)_nMg^{2+}$ and $(MgO)_nMg_2^{2+}$ have been detected by experiments of laser ionisation time of flight mass spectrometry [4,6]. The spectra show increased abundances of $(MgO)_{13}Mg^+$, $(MgO)_{13}Mg^{2+}$ and $(MgO)_{12}Mg_2^{2+}$ clusters. The first of these clusters was also observed by collision induced fragmentation analysis [1]. A simple explanation of these experimental features is that the cluster abundances are governed by their stabilities, which could result from the fact that they can be considered as pieces of the crystal lattice as an initial approximation. So $(MgO)_{13}Mg$ is the smallest $(MgO)_nMg$ cluster which involves a complete crystalline mesh. Besides, the smallest $(MgO)_nMg_2^{2+}$ experimentally observed, for $n = 12$ [4], can be interpreted as $(MgO)_{13}Mg$ with a double charged vacancy $V_0^{00}$. Computations based on a rigid ion model and *ab initio* Hartree-Fock calculations [4–6] seem to confirm the idea of clusters MgO constituted as modified pieces of the crystal lattice. (Similar conclusions were obtained on alkali-halides clusters which possess the same crystalline bulk structure [12–16].)

In this paper, the clusters $(MgO)_{13}Mg$ and $(MgO)_{12}Mg_2$ are studied with the help of *ab initio* procedures starting from the crystalline mesh of MgO.

[a] e-mail: coudray@lps.u-psud.fr

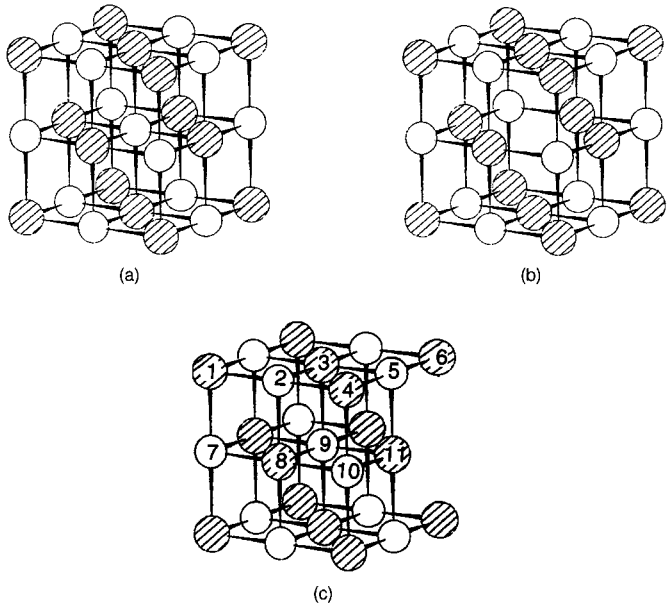


**Fig. 1.** Starting geometries of (a): $(MgO)_{13}Mg$; (b): cluster I with vacancy at the center of the cube; (c): cluster II with vacancy at the edge of the cube. The white circles are the oxygen atoms, the striped circles the magnesium atoms.

The disposition of the 27 atoms in $(MgO)_{13}Mg$ is unique, with three atoms along each edge of the cube. On the other hand, two configurations are possible in $(MgO)_{12}Mg_2$: the missing oxygen can be either at the center or on the edge of the cube (*cf.* Fig. 1). The first

structure will be called cluster I, the second one cluster II. The influence of the charge on the structure and stability of these clusters will be studied in details below. In particular, it will be shown that the vacancy location leading to the more stable cluster is charge dependent.

## 2 The numerical method

For our calculations, we have used the code DMol based on the theory of the functional density in the local density approximation (DFT-LDA theory) [17,18]. The program has been developed by Delley and was extensively described elsewhere [19,20]. The calculation is a two steps process. First, for a given geometry, DMol calculates the repartition of the electronic density which gives rise to the lowest total energy of the molecule with a precision of $10^{-6}$ a.u. The resulting forces acting on each atom are computed. Then, according to these forces, each atom is slightly moved, and an energy minimisation process starts again. The calculation stops when both energy variations and either forces or displacements become less than given values ($10^{-5}$ a.u. for energy variations and $10^{-3}$ a.u. for either forces or displacements).

In this study we have chosen a double numerical basis, in which the lowest orbitals of each atomic species, ($1s$ and $2s$ orbitals for Mg and $1s$ orbital for O) are frozen in order to reduce the computational time. The basis includes the other occupied orbitals in the neutral atom, *i.e.* the valence orbitals $2p$ and $3s$ of Mg, $2s$ and $2p$ of O plus $3d$ functions for both species in order to account for possible polarisation effects due to slight distortions (this basis set is usually called a DNP basis set). A $3s$ orbital relative to $Mg^{++}$ and two orbitals relative to $O^{++}$ ($2s$ and $2p$) are respectively added to the Mg and O sets [21]. To summarize, the basis sets read: $2p$, $3s$, $3s'$, $3d$ for Mg and $2s$, $2p$, $2s'$, $2p'$, $3d$ for O. With this basis, the numerical errors on the distances between atoms can be estimated to be of the order of 0.02 Å [20]. We have chosen the approximation of Hedin and Lundqvist [22] for the exchange and correlation energy, because it is well-adapted to computations concerning MgO [11,23,24].

The $Oh$ symmetry was chosen for $(MgO)_{13}Mg$ and for cluster I and the $C_{2V}$ symmetry for cluster II. These choices, which do not allow possible Jahn-Teller effects, are suggested by the experimental results previously quoted (Sect. 1). Besides, from a computational point of view, trials were made starting from initial geometries possessing lower symmetries; in any case the minimisations led us towards clusters possessing the highest symmetries.

## 3 Results

Starting from cube-like configurations for all clusters and imposing the previously described symmetries, the geometries of neutral and positively ionised clusters were computed. The cluster $(MgO)_{13}Mg^{Q+}$ which contains 27 atoms was calculated for $Q = 0, 1, 2$. The clusters $(MgO)_{12}Mg_2^{Q+}$ with an oxygen vacancy (clusters I and II) were calculated for $Q = 0, 1, 2, 3, 4$.

**Table 1.** Interatomic distances, in angströms and in atomic units, in (a): $[(MgO)_{13}Mg]^{Q+}$ and MgO crystal; (b): $[\text{cluster I}]^{Q+}$; (c): $[\text{cluster II}]^{Q+}$. In Table 1c, the two Mg atoms are those of the open edge in Figure 1, and the center of the cluster is defined as the intersection of the segments joining the opposite face magnesium.

(a)

| | | $Q=0$ | $Q=1$ | $Q=2$ | MgO crystal |
|---|---|---|---|---|---|
| $d_{Mg-Mg}$ | Å | 4.1 | 4.1 | 4.07 | 4.22 |
| opposite faces | a.u. | 7.75 | 7.75 | 7.70 | 7.97 |
| $d_{O-O}$ | Å | 5.77 | 5.76 | 5.76 | 5.97 |
| opposite edges | a.u. | 10.91 | 10.89 | 10.89 | 11.31 |
| $d_{Mg-Mg}$ | Å | 6.68 | 6.67 | 6.63 | 7.31 |
| opposite vertices | a.u. | 12.63 | 12.61 | 12.53 | 13.82 |

(b)

| | | $Q=0$ | $Q=1$ | $Q=2$ | $Q=3$ | $Q=4$ |
|---|---|---|---|---|---|---|
| $d_{Mg-Mg}$ | Å | 4.46 | 4.44 | 4.44 | 4.52 | 4.62 |
| opposite faces | a.u. | 8.43 | 8.39 | 8.39 | 8.54 | 8.73 |
| $d_{O-O}$ | Å | 5.64 | 5.64 | 5.64 | 5.60 | 5.55 |
| opposite edges | a.u. | 10.66 | 10.66 | 10.66 | 10.59 | 10.49 |
| $d_{Mg-Mg}$ | Å | 6.67 | 6.66 | 6.66 | 6.68 | 6.70 |
| opposite vertices | a.u. | 12.61 | 12.59 | 12.59 | 12.63 | 12.67 |

(c)

| | | $Q=0$ | $Q=1$ | $Q=2$ | $Q=3$ | $Q=4$ |
|---|---|---|---|---|---|---|
| $d_{Mg-Mg}$ | Å | 5 | 4.64 | 4.04 | 4.96 | 5.53 |
| open edge | a.u. | 9.45 | 8.77 | 7.64 | 9.38 | 10.45 |
| $d_{O\text{-center}}$ | Å | 0.01 | 0.02 | 0.05 | 0.12 | 0.16 |
| | a.u. | 0.02 | 0.04 | 0.09 | 0.23 | 0.30 |

### 3.1 Final geometries

Table 1 provides the computed distances between atoms and Figure 2, the final associated geometries. All distances in $(MgO)_{13}Mg$ are smaller than in the MgO crystal [25].

Removing the central oxygen atom in $(MgO)_{13}Mg$ causes a large increase (about 9%) of the $d_{Mg-Mg}$ distance between the magnesium atoms of opposite faces in cluster I (*cf.* Tabs. 1a and 1b), a decrease (less than 3%) of the distance between oxygen atoms of opposite edges, and a negligible variation of the farthest opposite vertices magnesium atoms. These deformations, which are represented for $Q = 0$ in Figure 3, lead to a "rounded" shape more pronounced for the vacancy cluster I than for the non vacancy cluster $(MgO)_{13}Mg$. The main tendencies in Figure 3 are still valid for higher $Q$ values.

The central oxygen atom in $(MgO)_{13}Mg$ fixes electrons which screen the repulsion between its first neighbours, the magnesium atoms of opposite faces. When the central atom is removed, electrons gather into the cluster (see Sect. 3). The screening effect is reduced and the increased repulsion between magnesium atoms of opposite faces pushes them outwards (*cf.* Fig. 3). Electrons carried

by the central oxygen atom, when it is present, have a repulsive effect on oxygen atoms of opposite edges. This repulsion decreases when the vacancy is created and oxygen atoms are brought closer. As to the magnesium atoms of the vertices, their third neighbours position with respect to the vacancy explains why their location remains almost fixed when the vacancy appears.

Cluster II deserves special attention due to its particular symmetry. First, the distance between Mg atoms located on the edge with the vacancy (open edge in Tab. 1c) is less than in the crystal for $Q = 2$. Second, the central oxygen atom moves toward the oxygen vacancy when $Q$ becomes greater than 2 (let us recall that the numerical error is about 0.02 Å).

In both clusters, the variations of distances with the charge $Q$ are extremely small, often at the limit of precision, when $Q$ increases from 0 to 2, but significant variations are observed when $Q$ becomes larger than 2 in cluster I.

### 3.2 Energies

Table 2 shows the total energies and the binding energies of the three clusters in the various charge states. The binding energy of a cluster is defined as the difference between its total energy and the energy of the isolated Mg and O neutral atoms. As expected it decreases when the positive charge $Q$ increases.

The energy necessary to extract an electron according to the following reaction:

$$(\mathrm{MgO})_n\mathrm{Mg}_p^{Q+} \rightarrow (\mathrm{MgO})_n\mathrm{Mg}_p^{(Q+1)} + e^- \qquad (1)$$

has been calculated in two ways in Table 3: the adiabatic ionisation potential $E_{\mathrm{ad}}$ given by the energy difference between two charge states $Q$ and $(Q+1)$ of Table 2 and the vertical ionisation potential $E_{\mathrm{v}}$ obtained when the electron is removed from the $(\mathrm{MgO})_n\mathrm{Mg}_p^{Q+}$ cluster, without

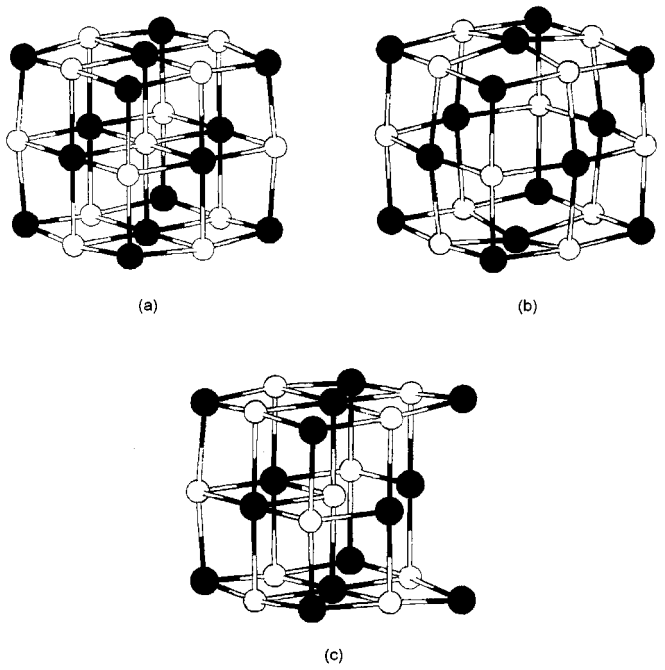


**Fig. 2.** Final geometries of (a): $(\mathrm{MgO})_{13}\mathrm{Mg}$; (b): cluster I; (c): cluster II. The white circles are the oxygen atoms, the black circles the magnesium atoms.

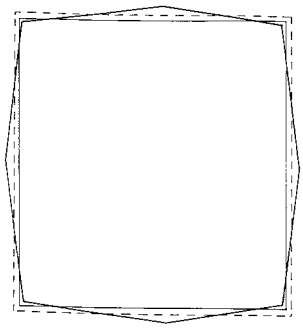

**Fig. 3.** Lattice deformation in the (100) central atomic plane in: the non-vacancy cluster for $Q = 0$ (thin line); the vacancy cluster I for $Q = 0$ (thick line); the dashed square represents the crystal lattice.

**Table 2.** Total energies $E_{\mathrm{tot}}$, and binding energies $E_{\mathrm{bind}}$ of the clusters, (a): $[(\mathrm{MgO})_{13}\mathrm{Mg}]^{Q+}$; (b): $[\text{cluster I}]^{Q+}$; (c): $[\text{cluster II}]^{Q+}$.

(a)

| | $Q=0$ | $Q=1$ | $Q=2$ |
|---|---|---|---|
| $E_{\mathrm{tot}}$ (a.u.) | −3 761.460 | −3 761.31 | −3 761.056 |
| $E_{\mathrm{bind}}$ (eV) | 124.65 | 120.60 | 113.66 |

(b)

| | $Q=0$ | $Q=1$ | $Q=2$ | $Q=3$ | $Q=4$ |
|---|---|---|---|---|---|
| $E_{\mathrm{tot}}$ (a.u.) | −3 686.524 | −3 686.386 | −3 686.148 | −3 685.756 | −3 685.257 |
| $E_{\mathrm{bind}}$ (eV) | 113.73 | 109.99 | 103.51 | 92.84 | 79.26 |

(c)

| | $Q=0$ | $Q=1$ | $Q=2$ | $Q=3$ | $Q=4$ |
|---|---|---|---|---|---|
| $E_{\mathrm{tot}}$ (a.u.) | −3 686.546 | −3 686.402 | −3 686.154 | −3 685.742 | −3 685.226 |
| $E_{\mathrm{bind}}$ (eV) | 114.35 | 110.42 | 103.68 | 92.45 | 78.41 |

**Table 3.** Values of $E_{ad}$ and $E_v$ adiabatic and vertical ionisation potentials of the clusters, (a): $[(MgO)_{13}Mg]^{Q+}$; (b): $[\text{cluster I}]^{Q+}$; (c): $[\text{cluster II}]^{Q+}$.

(a)

| | $Q=0$ | $Q=1$ |
|---|---|---|
| $E_{ad}$ (eV) | 4.05 | 6.94 |
| $E_v$ (eV) | 4.05 | 6.94 |

(b)

| | $Q=0$ | $Q=1$ | $Q=2$ | $Q=3$ |
|---|---|---|---|---|
| $E_{ad}$ (eV) | 3.74 | 6.48 | 10.67 | 13.54 |
| $E_v$ (eV) | 3.74 | 6.48 | 10.79 | 13.64 |

(c)

| | $Q=0$ | $Q=1$ | $Q=2$ | $Q=3$ |
|---|---|---|---|---|
| $E_{ad}$ (eV) | 3.96 | 6.74 | 11.23 | 14.05 |
| $E_v$ (eV) | 3.98 | 6.78 | 11.85 | 14.57 |

changing its geometry. As the adiabatic ionisation potential $E_{ad}$ takes into account the energy released by the relaxation of the $(MgO)_nMg_p^{(Q+1)}$ cluster, it is smaller than (or at least equal to) $E_v$. The difference between those two values is negligible for $Q=0$ and $Q=1$ (at the precision of the calculation, about 0.01 eV). For $Q=2$ and $Q=3$, $E_v - E_{ad}$ is about 0.1 eV in cluster I and 0.5 eV in cluster II.

### 3.3 Electronic densities

The Mulliken charges (*cf.* Tab. 4) represent the charges which can be attributed to each atom. They are not strictly localized around each atom due to the overlapping of atomic orbitals. Therefore they just provide a first estimate of the charge transfer, which is not strictly representative of ionicity. In all clusters, the values and the variations with $Q$ of these charges are very similar. The central oxygen atom, when it is present, carries the most important negative charge, about 1.5 electron, and is the less affected by the removal of electrons. The other oxygen atoms experience a slight increase of their negative charges when electrons are removed. At the same time, a large increase of the positive charge appears on the vertices of the magnesium atoms. This increase is particularly important in cluster II for the two atoms which belong to the vacancy edge. The positive charge of the faces magnesium atoms decreases when electrons are removed, with the exception of the first two neighbours of the vacancy in cluster II when $Q$ becomes greater than 2. Apart from this exception, it can be said that, the more the positive charge of a cluster increases, the more the electronic density concentrates on the edged oxygen and faced magnesium atoms, and the more the vertices magnesium atoms are depleted.

In Figure 4 the electronic density distributions of cluster I for the different charges are plotted along the direction [111]. These distributions show that the electronic density is very weak in the center of the vacancy. Starting from $Q=0$, the electronic charging of the vacancy first increases when the first two electrons are removed, then decreases very strongly with the removal of the last two, with a maximum for $Q=2$.

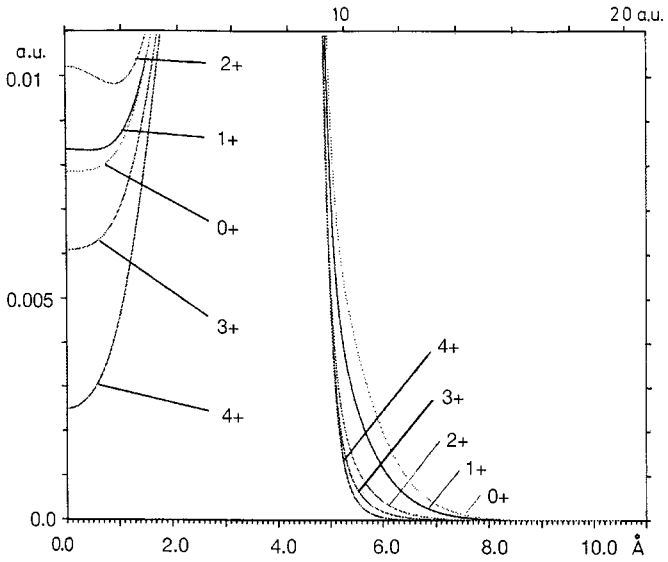


**Fig. 4.** Electronic densities along the central [111] axis of the oxygen vacancy cluster I. The origin is at the center of the oxygen vacancy. The numbers reported in the figure are the values of $Q$. The distances are given in angströms (lower scale) and in atomic units (upper scale), the electronic densities in electron per atomic unit cube.

In order to estimate the charge contained in the vacancy when $Q=2$, it is assumed that the vacancy is a sphere whose radius $r_v$ is deduced from the $d_{Mg-Mg}$ distance between its first two neighbours by the relation:

$$d_{Mg-Mg} = 2r_i^{Mg} + 2r_v \qquad (2)$$

in which $r_i^{Mg}$ is the ionic radius of magnesium. According to the charge attributed to this element, its ionic radius is 0.66 Å for $Mg^{++}$ and 0.82 Å for $Mg^{+}$ [26]. As the Mulliken charge of Mg has been found equal to 1.16 for $Q=2$ (*cf.* Tab. 4), it is appropriate to choose the radius $r_i^{Mg} =$ 0.82 Å, which leads to a vacancy radius $r_v$ of 1.4 Å, from equation (2) and Table 1. Then a charge of 0.89 electron is found in the vacancy sphere of 1.4 Å radius. However, when two electrons are removed, giving rise to a charge $Q=4$, the same sphere already contains 0.54 electron. This result means that, when the charge state is $Q=2$, only about a third of electron is brought into the vacancy by the addition of two electrons in the cluster.

On the external face of a vertice magnesium atom, the electronic density always decreases with $Q$ and gets closer to the atom, which corresponds to the increase of its positive charging (*cf.* Tab. 4b). On the external face of an oxygen atom, the situation is more complex: when $Q$ increases, the electronic density increases in the atomic core and decreases farther so the variations of the Mulliken

**Table 4.** Mulliken charges of the clusters, (a): $[(MgO)_{13}Mg]^{Q+}$; (b): [cluster I]$^{Q+}$; (c): [cluster II]$^{Q+}$. See Figure 1 for atoms locations.

(a)

| | $Q=0$ | $Q=1$ | $Q=2$ |
|---|---|---|---|
| central O | −1.46 | −1.47 | −1.50 |
| edge O | −1.29 | −1.31 | −1.34 |
| face Mg | 1.32 | 1.24 | 1.18 |
| vertice Mg | 1.13 | 1.34 | 1.56 |

(b)

| | $Q=0$ | $Q=1$ | $Q=2$ | $Q=3$ | $Q=4$ |
|---|---|---|---|---|---|
| central O | −1.30 | −1.31 | −1.33 | −1.36 | −1.39 |
| face Mg | 1.25 | 1.21 | 1.16 | 1.16 | 1.21 |
| vertice Mg | 1.01 | 1.19 | 1.37 | 1.53 | 1.67 |

(c)

| | $Q=0$ | $Q=1$ | $Q=2$ | $Q=3$ | $Q=4$ |
|---|---|---|---|---|---|
| Mg1 | 1.23 | 1.40 | 1.53 | 1.61 | 1.67 |
| Mg3 | 1.39 | 1.29 | 1.23 | 1.18 | 1.11 |
| Mg4 | 1.22 | 1.42 | 1.55 | 1.61 | 1.66 |
| Mg6 | 0.43 | 0.70 | 1.11 | 1.35 | 1.66 |
| Mg8 | 1.26 | 1.24 | 1.21 | 1.20 | 1.20 |
| Mg11 | 1.13 | 1.02 | 0.91 | 1.12 | 1.29 |
| O2 | −1.30 | −1.32 | −1.34 | −1.36 | −1.37 |
| O5 | −1.26 | −1.29 | −1.31 | −1.32 | −1.33 |
| O7 | −1.31 | −1.33 | −1.35 | −1.36 | −1.37 |
| O9 | −1.47 | −1.48 | −1.48 | −1.49 | −1.51 |
| O10 | −1.34 | −1.36 | −1.38 | −1.40 | −1.41 |

charge are less than for the previous magnesium atom (*cf.* Tab. 4b).

A precise comparison of these distributions when the charge state $Q$ is changing is not easy due to the modifications of the cluster geometry. So, instead of considering the "adiabatic" distributions depicted in Figure 4, we have computed "vertical" distributions obtained by removing one electron from a cluster without modifying its geometry. This procedure is justified by the small differences observed between the ionisation potentials $E_{ad}$ and $E_v$ (from negligible values to less than 0.7 eV), indicating weak relaxation effects. The difference between the vertical distributions for two different $Q$ states with $\Delta Q = +1$ has given rise to the maps of isodensity lines shown in Figures 5 and 6. One can infer from those outlines the reorganisation of the electronic density just after the positive ionisation of the cluster and before its relaxation. In a given region, a positive density difference indicates an increase of the electronic density just after the electron removal, while a negative one means an electronic density decrease.

## 4 Discussion

As one can see from Table 1, the $(MgO)_{13}Mg$ cluster slightly contracts when its positive charge increases. A

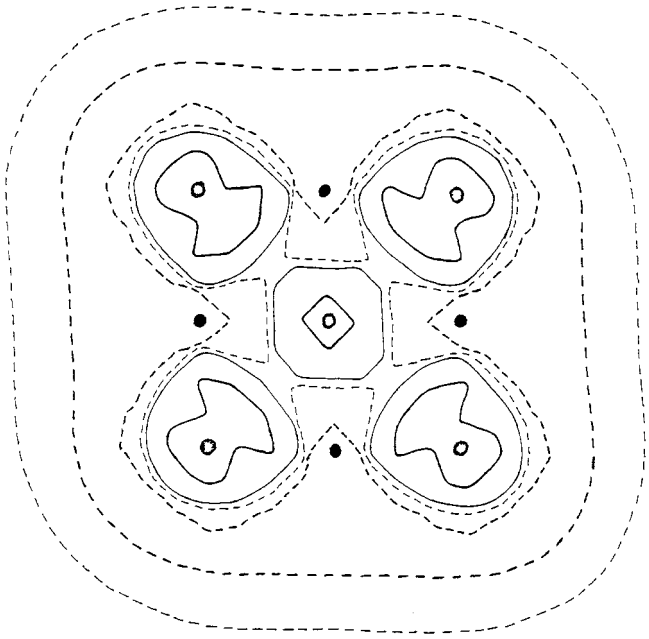

**Fig. 5.** "Vertical" variation of the electronic charge density in the central (100) plane of $(MgO_{13})Mg$ when the charge $Q$ varies from 0 to 1 (when $Q$ varies from 1 to 2 the variation is very similar). The white circles are the oxygen atoms, the black circles the magnesium atoms. Thick dashed line: $-10^{-4}$ $e/(\text{a.u.})^3$. Thin dashed line: $-3 \times 10^{-5}$ $e/(\text{a.u.})^3$. Thin continuous line: $10^{-5}$ $e/(\text{a.u.})^3$. Thick continuous line: $2 \times 10^{-4}$ $e/(\text{a.u.})^3$.

first explanation may be given by the Mulliken charges (*cf.* Tab. 4). As was previously mentioned in Section 3.3, when the molecule is positively ionised a global electronic density deficit appears which modifies the Mulliken charges of the atoms: oxygen atoms become more negatively charged, vertices magnesium atoms more positively, while other magnesium atoms experience a small decrease of their negative charge.

However the Mulliken charges do not give information on the local variations of the electronic density. These variations are given by the isodensity maps in Figures 5 and 6. In Figure 5, which shows the variations of the electronic charge when $Q$ varies from 0 to 1 in the central (100) plane of the non-vacancy cluster, the removed charge is mainly taken at the cluster surface and in the neighbourhood of magnesium atoms; furthermore, when the cluster looses one electron, the electronic density concentrates in the vicinity of oxygen atoms, which makes the cluster become more ionic. Conversely the addition of one electron in a positively charged cluster would increase its covalency character. All these modifications in the electronic density lead to variations of attractive forces between atoms: when one electron is removed, the attraction between each surface oxygen atom and its first four magnesium neighbours increases, and decreases slightly between the central oxygen and faces magnesium atoms. These variations lead to a small contraction of the cluster (*cf.* Fig. 3).

The shapes of cluster I and II cannot be directly compared due to their different symmetries. However,

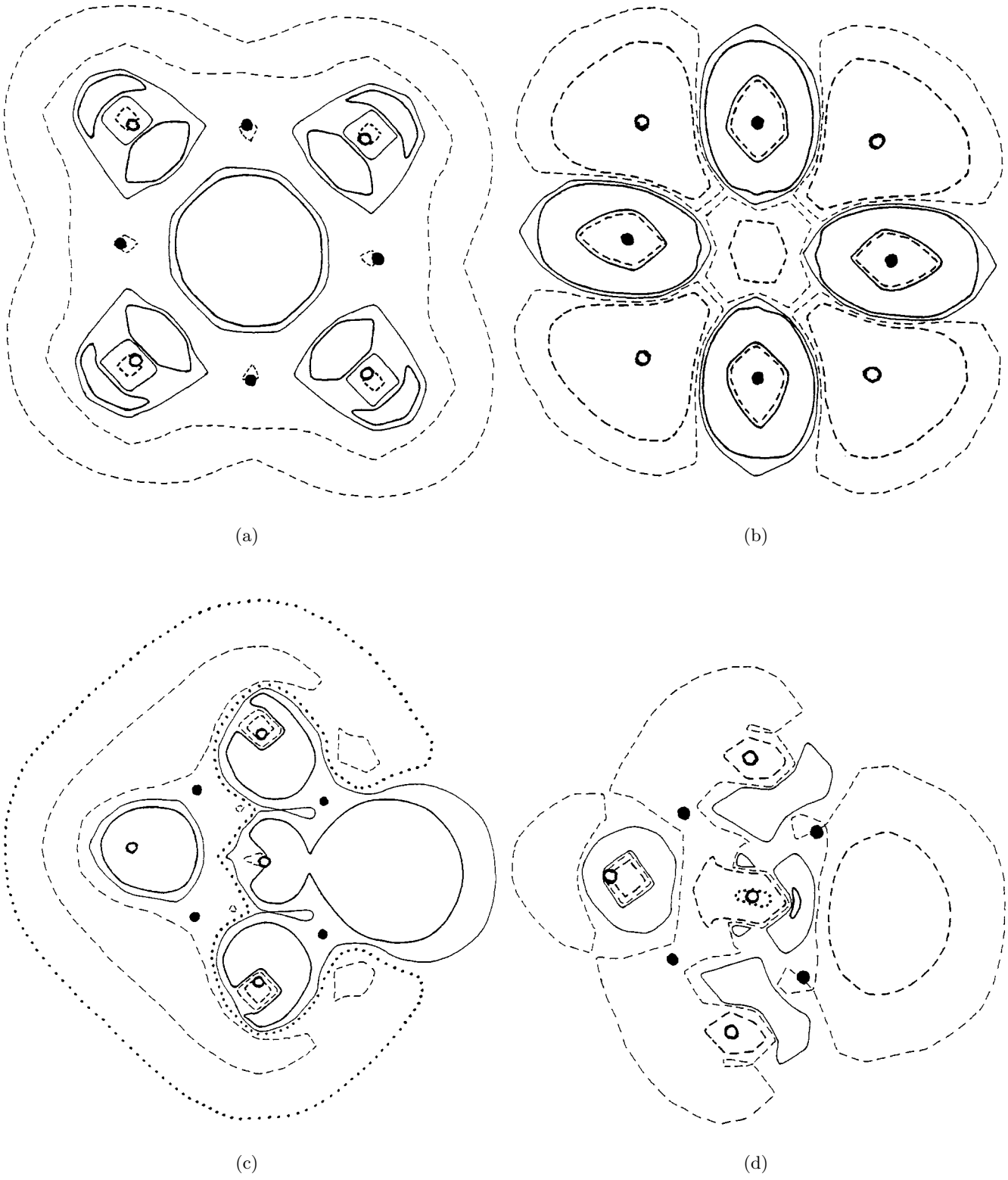


**Fig. 6.** "Vertical" variation of the electronic charge density in the central (100) plane of cluster I (a) and (b) and of cluster II (c) and (d). The charge $Q$ varies from 1 to 2 in (a) and (c) (similar variations from 0 to 1) and from 3 to 4 in (b) and (d) (similar variations from 2 to 3). The white circles are the oxygen atoms, the black circles the magnesium atoms. Dotted line: (d): $-10^{-2}$ $e/(\text{a.u.})^3$; thick dashed line: (a) $-10^{-3}$ $e/(\text{a.u.})^3$; (b) $-5\times10^{-3}$ $e/(\text{a.u.})^3$; (c) $-10^{-3}$ $e/(\text{a.u.})^3$; (d) $-10^{-3}$ $e/(\text{a.u.})^3$; thin dashed line (a) $-10^{-4}$ $e/(\text{a.u.})^3$; (b) $-10^{-3}$ $e/(\text{a.u.})^3$; (c) $-10^{-4}$ $e/(\text{a.u.})^3$; (d) $-10^{-4}$ $e/(\text{a.u.})^3$; dotted line: (c) $-2\times10^{-5}$ $e/(\text{a.u.})^3$; thin continuous line: (a) $5\times10^{-5}$ $e/(\text{a.u.})^3$; (b) $10^{-3}$ $e/(\text{a.u.})^3$; (c) $10^{-5}$ $e/(\text{a.u.})^3$; (d) $10^{-4}$ $e/(\text{a.u.})^3$; thick continuous line: (a) $10^{-4}$ $e/(\text{a.u.})^3$; (b) $5\times10^{-3}$ $e/(\text{a.u.})^3$; (c) $10^{-4}$ $e/(\text{a.u.})^3$; (d) $10^{-3}$ $e/(\text{a.u.})^3$.

a significant change in the evolution of the geometry of both clusters is observed between $Q = 2$ and $Q = 3$ (*cf.* Tab. 1). In cluster I, significant variations in the geometry appear for $Q$ greater than 2. In cluster II, the magnesium atoms belonging to the vacancy edge get closer from each other from $Q = 0$ to $Q = 2$, then, for $Q$ greater than 2, they move apart from each other. In correlation with this behaviour, the near central oxygen atom remains practically motionless from $Q = 0$ to $Q = 2$, then it is brought closer to the vacancy.

The variations of the electronic density in the central (100) plane of cluster I are represented in Figures 6a and 6b when the charge is respectively varying from $Q = 1$ to $Q = 2$ and from $Q = 3$ to $Q = 4$. Figure 6a shows that the variation of the charge density when one electron is removed consists of a decrease at the cluster periphery and an increase in the neighbourhood of any oxygen site – with or without atom –. These similarities explain the likeness of the evolutions of the Mulliken charges in cluster I from $Q = 0$ to $Q = 2$ and in $(MgO)_{13}Mg$ (*cf.* Tabs. 4a and 4b). It is worth noticing that in both cases no significant evolution of the geometries results from the variations of the localisation of the electronic charge (*cf.* Tabs. 1a and 1b). In Figure 6b the removing of one electron from $Q = 3$ to $Q = 4$ leads to a decrease of the charge density in the vacancy and in the immediate vicinity of atoms and to an increase of the charge density in between.

In Figures 6c and 6d which refer to cluster II the same trends as in cluster I are observed in the vacancy region for the charge density variations: a density enhancement when $Q$ varies from 1 to 2, and a depletion for $Q$ varying from 3 to 4.

When $Q$ varies from 1 to 2 in cluster II an electronic depletion appears at the cluster periphery as in cluster I, and the vacancy second neighbours oxygen atoms experience variations similar to those of cluster I (*cf.* Fig. 6a). Besides, each electron removed in cluster II gives rise to a shift of the remaining charge towards the vacancy region and in the neighbourhood of the oxygen atoms (*cf.* Fig. 6c). A fraction of this charge is taken on the first two vacant neighbouring magnesium atom positions. As a consequence these atoms are strongly attracted towards the vacancy, and this results into them getting closer to each other (*cf.* Tab. 1c). A similar process occurs in cluster I (*cf.* Tab. 1b). But the increase of the positive charge on the vertice magnesium atoms remains moderate, because the charge transfer is now shared between 6 atoms instead of 2 in cluster II. The consequence is that the variation of the distance between Mg atoms remains moderate.

Figures 6b and 6d illustrate the electronic depletion in the vacancy region which results from the removing of an electron from $Q = 3$ to $Q = 4$ in clusters I and II. A strong depletion appears in the immediate vicinity of the near central oxygen atom in cluster II (dashed region). In this cluster, the regions which gain some charge density are more or less located between oxygen and magnesium atoms, as in cluster I, and in the neighbourhood of the oxygen atom the farthest from the vacancy. The consequence of the electronic density loss of the vacancy is the enhanced repulsion of the two vacancy edge magnesium atoms, which increases the distance between them (*cf.* Tab. 1c). Similarly, the electronic depletion in the vacancy region of cluster I makes face magnesium atoms experience a weak increase of their positive charges, increasing slightly the distances between them (*cf.* Tab. 1b).

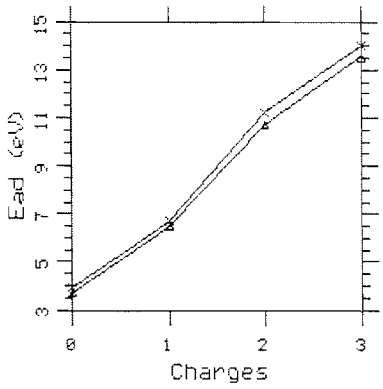


**Fig. 7.** Variation of the ionisation energy as a function of $Q$. The triangles refer to cluster I, the crosses to cluster II. The lines are only intended as a guide.

The discussion above has outlined the part played by the localisation of charges in the cluster geometry. This localisation has also an effect on the clusters ionisation energies. Table 3 shows that the removal of one electron requires more and more energy as $Q$ is increasing. It was shown in small $(NaF)_nNa$ clusters [27] that the magnitude of the ionisation potential could be associated with the localisation of the excess electron *i.e.* with the rank $n$ of the cluster (see also Ref. [28]). For instance when $(2n + 1)$ is the product of three integers the excess electron is highly delocalized and very low values of the ionisation potential ($\sim$ 2 eV) are obtained, intermediate values (3 to 4 eV) are obtained when $(2n + 2)$ is the product of three integers: the electron then sits in a vacancy in a way analogous to that of the bulk F-center; the other values of $n$ give rise to very high values ($> 5$ eV), and the electron is believed to neutralise the sodium cation. Although these calculations are carried out on neutral clusters composed of monovalent atoms, they show the same tendencies as ours. It is observed in Figure 4 that the positive ionisation of a neutral cluster ($Q = 0$) leads to an increase of the electronic density in the vacancy. This means that a delocalized electron has been removed from the cluster. The same scenario occurs when the charged cluster with $Q = 1$ is ionised. Following them, in the ionisation of clusters $Q = 2$ and $Q = 3$, an appreciable fraction of the electron localized in the vacancy is removed (*cf.* Fig. 4). This difference in the localisation of the removed electron can explain the variations of the ionisation energy as a function of $Q$ (*cf.* Fig. 7). For $Q = 2$ and 3, the ionisation energies are higher than expected from the continuation of the values obtained from $Q = 0$ and $Q = 1$. The localisation of an electron close to a magnesium atom, as it was done in reference [29] for sodium, cannot be studied in the present case, due to the fourfold symmetry of the simulation.

It is interesting to notice that in the three clusters studied, the values $E_v$ and $E_{ad}$ are very comparable. This similarity results from a delocalisation of the removed electron in all clusters.

A question of great interest is the problem of the stable location of the vacancy according to the charge of the cluster. The binding energies in Table 2 indicate that the most stable structure is that of cluster II for $Q = 0, 1, 2$ and that of cluster I for $Q = 3$ and 4. Comparable results [15] were obtained on $[(NaF)_{12}Na_2]^{Q+}$ clusters in which, as in the present simulation, cube-like structures were assumed (rocksalt structure of the crystalline NaF and $[(NaF)_{12}Na]^+$ clusters abundances in the experimental mass spectra). In these clusters, the most stable structure corresponds to cluster II when $Q = 0$ and $Q = 1$ and to cluster I for $Q = 2$. Similarly, in another computation, $[(NaCl)_{12}Na_2]^{2+}$ was found stabilized in cluster I [30]. The fact that the transition holds for $Q = 1$ for NaF instead of $Q = 2$ for MgO is likely to be due to the difference of the valences of the anions involved. Hence for NaF as for MgO clusters, starting from a neutral cluster and removing electrons successively, the vacancy location leading to the more stable structure is at first on the edge of the cluster and then in its center. In our computation, as in reference [15], the transition appears when the number of electrons removed is greater than the missing anion valence.

Conversely, starting from an ionic cluster $[(MgO)_{13}Mg]^{2+}$ (resp. $[(NaF)_{13}Na]^+$), in which a $2^+$ oxygen vacancy (resp. a $1^+$ fluorine vacancy) is created to form a $[(MgO)_{12}Mg_2]^{4+}$ cluster (resp. a $[(NaF)_{12}Na_2]^{2+}$ cluster), and introducing electrons successively in it, the vacancy location would be the center of the cluster as long as the number of added electrons is less than the missing anion vacancy; otherwise it would be the center of an edge. In other words, as long as the missing charge due to the anion vacancy is not compensated, the vacancy "prefers" the center of the cluster; when the missing charge is compensated the edge is favoured.

The charge compensation of the vacancy corresponds to a phase transition with a symmetry breaking. Then, as was previously quoted, it is not surprising that charge densities, interatomic distances and ionisation potentials experience drastic variations at the charge compensation.

With the help of a rigid ion model, Ziemann and Castleman have shown [4] that $(MgO)_n$ clusters prefer cubic geometries if a valence 1 is assumed for each atom, and spherical structures for a valence equal to 2. This can be interpreted as a relation between the surface to volume ratio and the ionicity: this ratio is at its minimum when the ionicity is at its maximum. These results cannot be directly compared with those from the present study, in which ionicity varies with $Q$. Now, in regard to the stability of the high cluster values of $Q$ are associated with a closed structure (vacancy in the center), and lower values with an open structure (vacancy on one edge). In the second structure, the surface to volume ratio is obviously higher than in the first one which presents a more spherical shape. Simultaneously, the first structure is associated with a greater ionicity than the second one as can be observed for most atoms in Tables 4b and 4c.

The $(2 \times 13)$ $2p$-type states relative to oxygen atoms in the cluster $[Mg_{14}O_{13}]^{2+}$ are filled with $(2 \times 14)$-2 valence electrons of magnesium atoms. Thus, at zero absolute temperature, the $2p$-type oxygen states are completely filled with electrons as the $2p$ band of the neutral MgO crystal. This means that the cluster $[Mg_{14}O_{13}]^{2+}$ is equivalent to the MgO crystal as regard to the electronic properties. Removing the central oxygen atom leaves two valence electrons of magnesium atoms in excess. The vacancy cluster $[Mg_{14}O_{12}V_0]^{2+}$ is obtained, in which $V_0$ denotes the oxygen vacancy. The vacancy formation energy $E_f$ is defined as the energy difference between the neutral crystal containing one vacancy plus the neutral oxygen atom located at infinity, and the perfect neutral crystal. Its value can be deduced from the binding energies of $[Mg_{14}O_{13}]^{2+}$ and $[Mg_{14}O_{12}V_0]^{2+}$ given in Table 2. The result is slightly different according to the position of the vacancy: in cluster I $E_f = 10.16$ eV and in cluster II $E_f = 10.01$ eV. These values are very similar to those of Kantorovich *et al.* [24], who obtained 10.55 eV in the bulk of MgO crystal, and 9.56 at the (100) surface, and to those of Castanier and Noguera [31] who obtained 9.95 eV at the same MgO surface.

Another comparison can be done with the cohesive energy of crystalline MgO, for which the experimental value is 10.5 eV/molecule [32]. To get an estimate of the cohesive energy in clusters which contain 14 Mg atoms and 13 O atoms, we proceed by adding the binding energy of a neutral oxygen atom (which is equal to $E_f$) to the binding energy of $[Mg_{14}O_{13}]^{2+}$ and then by dividing the result by the number of molecules so obtained. This leads to 8.84 eV/molecule for cluster I, and to 8.12 eV/molecule for cluster II. The difference with the experimental value in the crystal is due to the surface to volume ratio, which is larger in cluster II than in cluster I.

## 5 Conclusion

In the vacancy cluster $[Mg_{14}O_{12}V_0]^{2+}$ – equivalent to the MgO crystal with a neutral oxygen vacancy and two valence electrons in excess –, only a low fraction of electrons is contained in a vacancy of radius 0.14 nm (Sect. 3.3), which leads to the following sharing of charge:

$$[Mg_{14}O_{12}V_0]^{2+} \leftrightarrow \left[[Mg_{14}O_{12}]^{(2+)}\right]^{+\varepsilon} + [V_0]^{-\varepsilon}$$

with $\varepsilon \cong 0.35$.

In other words, the two electrons in excess do not remain on the oxygen vacancy site but spread all over the cluster.

Removing a neutral oxygen atom from a crystal can consist of removing an oxygen ion $O^{2-}$ which leaves the crystal in a $2^+$ state, and then of neutralising it by the reinjection of 2 electrons. Formally this process can be written as follows:

$$[nMg + (n-1)O + V_0]^{2+} + 2 \text{ electrons}$$

which is more conventionally written as:

$$[n\mathrm{Mg} + (n-1)\mathrm{O} + 2 \text{ electrons}] + \mathrm{V}_0^{2+}$$

in which the charge $2^+$ is generally attributed to the oxygen vacancy. In fact, in a crystal the oxygen vacancy which constitutes a F center [33] can accept a part of the two reinjected electrons, so that the following structural equation is obtained:

$$[n\mathrm{Mg} + (n-1)\mathrm{O}]^{(2-)+\varepsilon'} + \mathrm{V}_0^{(2+)-\varepsilon'}$$

in which $\varepsilon'$ is the electron charge trapped in the vacancy and $\varepsilon'-2$ the complementary electron charge spread over the crystal. Usually three charge states $F^{2+}$, $F^+$ and F [34] are considered, which correspond respectively to $\varepsilon' = 0, 1, 2$.

In alumina crystals the state of lowest energy is $F^+$, that is an oxygen vacancy with one electron ($\varepsilon' = 1$) [35]. In MgO crystals it was found that the stable state was F with $\varepsilon' = 2$ [36], but more recent calculations give $F^+$ with $\varepsilon' = 1$ [37]. Our computation leads to $\varepsilon' = 0.89$ in the oxygen vacancy of the neutral cluster $[Mg_{14}O_{12}V_0]^{2+}$, which is a value comparable to that mentioned in the last reference. These values suggest that an oxygen vacancy embedded in a neutral MgO medium is in the electronic state $F^+$. The study underway of clusters comprising 125 atoms would probably give more information on that point.

In the Appendix are quoted the states relative to the HOMO and to the LUMO in each cluster. It must be noticed that (i) the symmetry gives rise to partially occupied HOMO shells in cluster I for $Q = 1$ and $Q = 0$, and in cluster II for $Q = 3$ and (ii) as can be foreseen, when the HOMO shells relative to the cluster $Q = q+1$ are partially filled the added electron leading to cluster $Q = q$ sits in the same HOMO shells; when they are filled it sits in an orbital of same symmetry as the LUMO shell relative to cluster $Q = q + 1$.

The Mulliken charges do not generally provide a direct access to the ionicity of atoms, because they contain the atomic overlap integrals. However in the present case, these integrals are small, about a few atom percent, and the Mulliken charges provide a good estimate of the charges which can be attributed to each atomic species, that is about 1.3 to 1.5 electron on oxygen atoms, and 0.5 to 0.8 on magnesium atoms. Therefore the ionicity of atoms is always less than it could be foreseen from the valence 2 generally accorded to oxygen and magnesium atoms. Furthermore, ionicity depends on the coordination of the atom and varies with the total charge $Q$ of the cluster. The main result is that the variations of ionicity with $Q$ are more important on magnesium than on oxygen atoms. These variations increase when the coordinence of the atom decreases. In the study of bigger clusters underway, the variations of ionicity with $Q$ seem to confirm these results.

The last point to be mentioned is the phase transition associated with the stable location of the oxygen vacancy which passes from the centre of the cluster when it is highly charged, $Q = 4, 3$, to the edge when $Q = 2, 1, 0$. As any phase transition this one implies a symmetry breaking which causes a "rupture" in the properties, (charge densities, interatomic distances and morphology, and ionisation potentials). This phase transition appears when the cluster charge is such that its electronic properties are equivalent to those of a neutral crystal.

Biosym Technologies are acknowledged for the use of the computational method DMol. The authors are very grateful to Drs. M. Gupta and E. Wimmer for many helpful discussions and suggestions.

## Appendix

The state symbols relative to the HOMO and to the LUMO are given in Tables 5–7. For the HOMO, the occupation number of each state is given in parenthesis.

**Table 5.** Non vacancy cluster.

| | $Q = 0$ | $Q = 1$ | $Q = 2$ |
|---|---|---|---|
| HOMO | $1a_{1g}\uparrow(1)$, $1a_{1g}\downarrow(1)$ | $1a_{1g}\uparrow(1)$ | $1a_{2g}\uparrow(1)$, $1a_{2g}\downarrow(1)$ |
| LUMO | $1, 2, 3t_{1u}\uparrow\downarrow$ | $1a_{1g}\downarrow$ | $1a_{1g}\uparrow\downarrow$ |

**Table 6.** Cluster I.

| | $Q = 0$ | $Q = 1$ | $Q = 2$ | $Q = 3$ | $Q = 4$ |
|---|---|---|---|---|---|
| HOMO | $1t_{1u}\uparrow(2/3)$, $2t_{1u}\uparrow(2/3)$, $3t_{1u}\uparrow(2/3)$ | $1t_{1u}\uparrow(1/3)$, $2t_{1u}\uparrow(1/3)$, $3t_{1u}\uparrow(1/3)$ | $1a_{1g}\downarrow(1)$ | $1a_{1g}\uparrow(1)$ | $1t_{2u}\uparrow(1)$, $2t_{2u}\uparrow(1)$ $3t_{2u}\uparrow(1)$, $1t_{2u}\downarrow(1)$ $2t_{2u}\downarrow(1)$, $3t_{2u}\downarrow(1)$ |
| LUMO | $t_{2g}\uparrow$ | $1, 2, 3t_{1u}\downarrow$ | $1, 2, 3t_{1u}\uparrow\downarrow$ | $1a_{1g}\downarrow$ | $1a_{1g}\uparrow\downarrow$ |

**Table 7.** Cluster II.

| | $Q = 0$ | $Q = 1$ | $Q = 2$ | $Q = 3$ | $Q = 4$ |
|---|---|---|---|---|---|
| HOMO | $1a_1\uparrow(1)$ | $1b_1\uparrow(1)$ | $1a_1\uparrow(1)$ $1a_1\downarrow(1)$ | $1a_1\uparrow(1/2)$ $1a_1\downarrow(1/2)$ | $1b_2\uparrow(1)$ $1b_2\downarrow(1)$ |
| LUMO | $1b_2\uparrow$ | $1a_1\uparrow$ | $1b_1\uparrow\downarrow$ | $1b_1\uparrow\downarrow$ | $1a_1\uparrow\downarrow$ |

## References


1. W.A. Saunders, Phys. Rev. B **37**, 6583 (1988).
2. W.A. Saunders, Z. Phys. D **12**, 601 (1989).
3. T.P. Martin, T. Bergmann, J. Chem. Phys. **90**, 664 (1989).
4. P.J. Ziemann, A.W. Castleman Jr, J. Chem. Phys. **94**, 718 (1991).
5. P.J. Ziemann, A.W. Castleman Jr, Phys. Rev. B **44**, 6488 (1991).
6. P.J. Ziemann, A.W. Castleman Jr, Z. Phys. D **20**, 97, (1991).
7. P.J. Ziemann, A.W. Castleman Jr, J. Phys. C **96**, 4271 (1992).
8. C. Bréchignac, Ph. Cahuzac, F. Carlier, M. de Frutos, J. Leygnier, J.Ph. Roux, J. Chem. Phys. **99**, 6848 (1993).
9. J.M. Recio, A. Ayuela, R. Pandey, A.B. Kunz, Supp. Z Phys. D **26**, 237 (1993).
10. M. Recio, R. Pandey, A. Ayuela, A.B. Kunz, J. Chem. Phys. **98**, 4783 (1993).
11. S. Veliah, R. Pandey, Y.S. Li, J.M. Newsam, B. Vessal, Chem. Phys. Lett. **235**, 53 (1995).
12. C. Ochsenfeld, R. Ahlrichs, J. Chem. Phys. **97**, 3487 (1992).
13. T.P. Martin, J. Chem. Phys. **69**, 2036 (1978).
14. N.G. Phillips, C.W.S. Conover, L.A. Bloomfield, J. Chem. Phys. **64**, 4980 (1991).
15. G. Rajagopal, R.N. Barnett, U. Landman, Phys. Rev. Lett. **67**, 727 (1991).
16. P. Xia, Naichang Yu, L.A. Bloomfield, Phys. Rev. B **47**, 10040 (1993).
17. P. Hohenberg, W. Kohn, Phys. Rev. B **136**, 864 (1964).
18. W. Kohn, L.J. Sham, Phys. Rev. A **140**, 1133 (1965).
19. B. Delley, J. Chem. Phys. **92**, 508 (1990).
20. B. Delley, J. Chem. Phys. **94**, 7245 (1991).
21. B. Delley, A.J. Freeman, M. Weinert, E. Wimmer, Phys. Rev. B **27**, 6509 (1983).
22. L. Hedin, B.I. Lundqvist, J. Phys. C **4**, 2064 (1971).
23. A.J. Freeman, E. Wimmer, Ann. Rev. Mater. Sci. **25**, 7 (1995); M. Eto, Physica B **194**, 1565 (1994); U. Schönberger, F. Aryasetiawan, Phys. Rev. B **52**, 8788 (1995).
24. L.N. Kantorovich, J.M. Holender, M.J. Gillan, Surf. Sci. **343**, 221 (1995).
25. K.J. Chang, M.L. Cohen, Phys. Rev. B **30**, 4774 (1984).
26. *C.R.C. Handbook of Chemistry and Physics*, 72nd edn. (CRC Press, Boca Raton, 1992), Table 12-8.
27. P. Labastie, J.M. L'Hermite, Ph. Poncharal, M. Sence, J. Chem. Phys. **103**, 6362 (1995).
28. R.N. Barnett, U. Landman, C.L. Cleveland, J. Jortner, Phys. Rev. Lett. **59**, 811 (1987).
29. J. Giraud-Girard, D. Maynau, Z. Phys. D **32**, 255 (1994).
30. T.P. Martin, Phys. Rep. **95**, 167 (1983).
31. E. Castanier, C. Noguera, Surf. Sci. **364**, 1 (1996).
32. F. Seitz, *The modern theory of solids* (Mac Graw Hill, New York, 1940). Table XII, p. 48.
33. C. Kittel, *Introduction to solid state physics*, 3rd edn. (John Wiley and Sons, New York, 1968), pp. 571–587.
34. Q.S. Wang, N.A.W. Holzwarth, Phys. Rev. B **41**, 3211 (1990).
35. A. Stashaus, E. Kotomin, J.L. Calais, Phys. Rev. B **49**, 14854 (1994).
36. B.D. Evans, G.J. Pogatshnik, Y. Chen, Nucl. Instrum. Meth. Phys. Res. B **91**, 258 (1994).
37. M. Gupta, private communication.